proteins to be orthologous only if they are mutual best matches by BLAST and map to regions of conserved synteny, as determined by DNA sequence–based anchors (see text), between the mouse and human genomes. In addition, we include in our analysis only the class of paralogs that are the result of local gene duplication in one or the other species. We are aware that this is a narrow view of these concepts but use it here for the sake of clarity.
36. J. C. Auffray, P. Fontanillas, J. Catalan, J. Britton-Davidian, *J. Hered.* **92**, 23 (2001).
37. R. H. Reeves *et al.*, *Nature Genet.* **11**, 177 (1995).
38. H. Sago *et al.*, *Proc. Natl. Acad. Sci. U.S.A.* **95**, 6256 (1998).
39. M. T. Pletcher, T. Wiltshire, D. E. Cabin, M. Villanueva, R. H. Reeves, *Genomics* **74**, 45 (2001).
40. From the Jackson Laboratory maps, NCBI site maps, Oxford grids, and Annual Human Genome Project Report maps (www.informatics.jax.org/menus/map_menu.shtml, www.ncbi.nlm.nih.gov/Homology/, www.informatics.jax.org/searches/oxfordgrid_form.shtml, and www.ornl.gov/hgmis/research/mapping.html, respectively).
41. J. L. Doyle, U. DeSilva, W. Miller, E. D. Green, *Cytogenet. Cell Genet.* **90**, 285 (2000).
42. P. Dehal *et al.*, *Science* **293**, 104 (2001).
43. B. F. Koop, *Trends Genet.* **11**, 367 (1995).
44. S. Zoubak, O. Clay, G. Bernardi, *Gene* **174**, 95 (1996).
45. S. J. O'Brien *et al.*, *Science* **286**, 458 (1999).
46. B. John, G. L. Miklos, *Eukaryote Genome in Development and Evolution* (Allen & Unwin, Boston, 1988).
47. J. H. Nadeau, B. A. Taylor, *Proc. Natl. Acad. Sci. U.S.A.* **81**, 814 (1984).
48. J. H. Nadeau, D. Sankoff, *Nature Genet.* **15**, 6 (1997).
49. A. M. Mallon *et al.*, *Genome Res.* **10**, 758 (2000).
50. R. J. Britten, E. H. Davidson, *Q. Rev. Biol.* **46**, 111 (1971).
51. P. Soriano, G. Macaya, G. Bernardi, *Eur. J. Biochem.* **115**, 235 (1981).
52. D. J. Griffiths, *Genome Biol.* **2**, 1017 (2001).
53a. A number of papers have been published by users of the Celera mouse data (*62–65*).
53b. M. F. Festing, in *Genetic Variants and Strains of the Laboratory Mouse*, M. Lyon *et al.*, Eds. (Oxford Univ. Press, Oxford, 1996), pp. 1537–1576.
54. E. M. Simpson *et al.*, *Nature Genet.* **16**, 19 (1997).
55. D. W. Threadgill *et al.*, *Mamm. Genome* **8**, 390 (1997).
56. M. F. Festing *et al.*, *Mamm. Genome* **10**, 836 (1999).
57. S. F. Altschul, W. Gish, W. Miller, E. W. Myers, D. J. Lipman, *J. Mol. Biol.* **215**, 403 (1990).
58. E. C. Uberbacher, Y. Xu, R. J. Mural, *Methods Enzymol.* **266**, 259 (1996).
59. C. Burge, S. Karlin, *J. Mol. Biol.* **268**, 78 (1997).
60. R. J. Mural, *Methods Enzymol.* **303**, 77 (1999).
61a. A. A. Salamov, V. V. Solovyev, *Genome Res.* **10**, 516 (2000).
61b. S. Kumar, S. Subramanian, *Proc. Natl. Acad. Sci. U.S.A.* **99**, 803 (2002).
62. I. Rodriguez *et al.* *Nature Neurosci.* **5**, 134 (2002).
63. D. A. Sierra *et al.*, *Genomics* **79**, 177 (2002).
64. X. Zhang, S. Firestein, *Nature Neurosci.* **5**, 124 (2002).
65. J. M. Young *et al.*, *Hum. Mol. Genet.* **11**, 535 (2002).
66. J. F. Abril, R. Guigo, *Bioinformatics* **16**, 743 (2000).
67. We thank additional members of Celera's DNA sequencing, software, and IT groups for their valuable contributions to this work.

20 December 2001; accepted 29 April 2002

REPORTS

Explaining the Latitudinal Distribution of Sunspots with Deep Meridional Flow

Dibyendu Nandy and Arnab Rai Choudhuri

Sunspots, dark magnetic regions occurring at low latitudes on the Sun's surface, are tracers of the magnetic field generated by the dynamo mechanism. Recent solar dynamo models, which use the helioseismically determined solar rotation, indicate that sunspots should form at high latitudes, contrary to observations. We present a dynamo model with the correct latitudinal distribution of sunspots and demonstrate that this requires a meridional flow of material that penetrates deeper than hitherto believed, into the stable layers below the convection zone. Such a deep material flow may have important implications for turbulent convection and elemental abundance in the Sun and similar stars.

The 11-year cycle of sunspots was discovered about 150 years ago (*1*); the magnetic nature of this solar cycle became apparent about 100 years ago (*2*), and hydromagnetic dynamo theory to explain the origin of this cycle was developed about 50 years ago (*3*). Still, to this date, we do not have a solar dynamo model that explains different aspects of the solar cycle in detail. An understanding of the complex plasma motions and the conditions that exist within the turbulent solar convection zone (SCZ) is essential for building any model of the solar dynamo (*4, 5*). Even a decade ago, our knowledge about the solar interior was too limited to develop a realistic dynamo model. The following developments within the past few years have drastically changed the scenario.

Helioseismology has mapped the angular velocity distribution $\Omega(r,\theta)$ in the solar interior (*6, 7*) (Fig. 1) and has discovered the tachocline—a region of substantial radial shear ($d\Omega/dr$) in the rotation at the base of the SCZ. There the strong toroidal magnetic field is produced (as a result of the stretching of poloidal field lines) and then rises radially (as a result of magnetic buoyancy) to form sunspots. Simulations of this buoyant rise have established that the strength of the "sunspot-forming" toroidal field at the base of the SCZ must be on the order of 10^5 G (*8–10*). The classical α-effect (*3, 5*), which involves the twisting of the toroidal field by helical turbulence to produce the poloidal field, cannot affect such a strong field. Therefore, the most likely mechanism for the generation of the poloidal field (the weak "diffuse" field observed on the solar surface outside of sunspots) is the decay of tilted sunspot pairs on the solar surface (*11, 12*). This mechanism can be incorporated in kinematic dynamo models by invoking an α-effect concentrated in a thin layer near the solar surface (*13–16*). The meridional circulation of the Sun carries the weak poloidal field generated at the solar surface (by this α-effect) first poleward and then downward to the tachocline, where it can be stretched to produce the toroidal field (*13–19*).

Although a meridional flow of material toward the poles is observed in the outer 15% of the Sun (*20, 21*), nothing much is known about the counterflow toward the equator, except that it must exist to conserve mass. This flow is driven by turbulent stresses in the SCZ, and standard theories of convection suggest a flow that is contained mainly within the SCZ. When kinematic models of the solar dynamo include such a flow (black contours with arrows in Fig. 1), a helioseismically determined rotation profile, and an α-effect concentrated near the solar surface, such models tend to produce strong magnetic fields at higher latitudes (*14, 15, 19*). A buoyancy algorithm that we have constructed (*16, 22*), when included in such a model, results in sunspots at polar latitudes (Fig. 2A). The radial shear in the differential rotation $d\Omega/dr$ within the tachocline, which has opposite signs at higher and lower latitudes (Fig. 1), has larger amplitude at high latitudes. This results in the toroidal field being produced predominantly at high latitudes in the tachocline (from the poloidal field that has been dragged down by the meridional downflow near the poles), giving rise to sunspots there. Even in solar interface dynamo models, a solar-like rotation tends to produce non–solar-like solutions (*23*).

These results are insensitive to the strength of the α-effect, nor do they change qualitatively if we change the value of the turbulent diffusivity in the SCZ. The situation does not improve if one tries to evade the negative radial shear in the tachocline at high latitudes with a counterflow that is contained within the SCZ at high latitudes and enters the tachocline at low latitudes only. It turns out that the latitudinal shear within the SCZ at high latitudes is strong

Department of Physics, Indian Institute of Science, Bangalore 560012, India. E-mail: dandy@physics.iisc.ernet.in, arnab@physics.iisc.ernet.in

enough to produce stronger magnetic fields there, as compared to the positive radial shear in the tachocline at low latitudes (*24*). Attempts have also been made to avoid stronger activity at high latitudes by artificially suppressing the α-effect there (*14, 15*). Although this decreases the activity at high latitudes to some extent, it fails to solve the problem completely. Strong magnetic fields and sunspot eruptions at high latitudes are thus hard to avoid with a meridional flow confined to the tachocline and above.

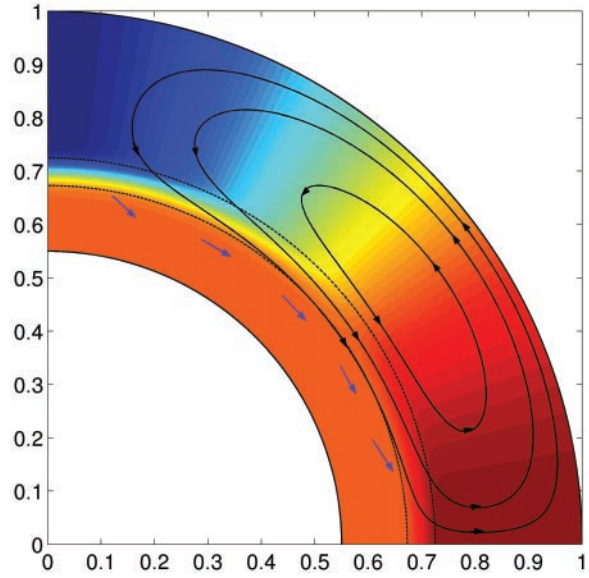

Fig. 1. Meridional cut of the Sun corresponding to the geometry of our simulation. Various colors represent the internal rotation as inferred from helioseismology (*6, 7*). In the solar convection zone, which occupies the outer 30% of the Sun, the rotation rate increases from a lower value at the pole (deep blue) to a higher value at the equator (dark red). The radiative interior of the Sun rotates uniformly (orange region) and has much less turbulence. The tachocline is the thin region (of thickness 0.05*R*, where R = solar radius) of strong radial shear (between the dashed lines) across which the latitude-dependent rotation of the SCZ changes over to the uniform rotation of the interior. In our model, the turbulent convection zone has a high diffusivity on the order of 10^8 m^2/s, with the diffusivity falling rapidly but smoothly within the tachocline to a value three orders of magnitude less in the radiative region. A meridional flow confined to the tachocline and above (represented by streamlines with arrowheads marking the direction of circulation) leads to sunspot formation at high latitudes. However, a deeper flow (indicated by arrows) penetrating below the tachocline (streamlines of such a flow are shown in Fig. 3A) generates sunspots at low latitudes, as observed. The flow amplitude is taken to be 20 m/s at the surface (*20*). Our computation domain corresponds to the northern hemisphere of the Sun, extending from latitudes 0° (equator) to 90° (pole) and from 0.55*R* (in the radiative interior) to the solar surface. We take a positive α-effect (which represents the mechanism of poloidal field generation from the decay of sunspots) concentrated between 0.95*R* and *R* and with an angular dependence of cos θ.

A meridional flow of material that penetrates beneath the SCZ and the tachocline into the stable radiative layers below (Fig. 3A) can resolve the above problem. In this case, the toroidal field created at high latitudes is dragged down immediately into the stable region by the meridional downflow there. A horizontal magnetic field becomes buoyant if it is at or above the base of the SCZ, where the temperature gradient is either nearly adiabatic or superadiabatic. But its buoyancy can be suppressed (*25, 26*) if it is put in the subadiabatic stable interior just beneath the tachocline. The strong magnetic field produced at high latitudes cannot erupt there if it is pushed down into the stable layers by the penetrating meridional downflow. Subsequently, the counterflow transports it equatorward through this stable region. Only when the meridional flow rises at low latitudes can the toroidal field come out through the base of the SCZ and be subject to magnetic buoyancy, erupting outward to form sunspots. This scenario, shown explicitly through the results of our dynamo simulations (*22*) in Figs. 2B and 3, is remarkably successful in giving a consistent description of the observations of sunspots at low latitudes in light of recent developments.

According to conventional wisdom, the toroidal field that produces sunspots at low latitudes is generated at the low latitude itself. In contrast, our results show that the strong toroidal field is actually generated above 45° latitude but is allowed to come out into the SCZ and erupt only at low latitudes.

It is not immediately obvious what physical

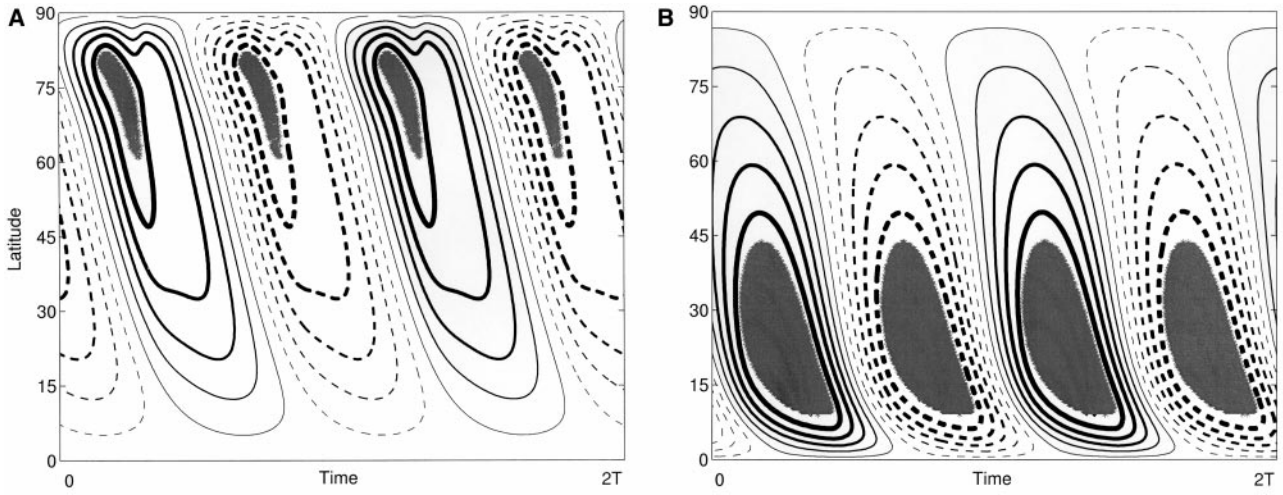

Fig. 2. An eruption latitude versus time plot of sunspots is traditionally called a butterfly diagram. To compare with observations, we construct theoretical butterfly diagrams showing the values of the toroidal magnetic field at the base of the SCZ (at 0.71*R*) over two dynamo periods *T* (equivalent to four sunspot cycles). Solid and dashed contours represent positive and negative values of the magnetic field, respectively, with thicker contours depicting stronger fields. A buoyancy formulation (*16, 22*) is built into the model, wherein toroidal magnetic fields exceeding 10^5 G above the base of the convection zone (but not below) erupt radially outward to the surface, simulating sunspot formation. Overlaid on the magnetic field contours are gray regions denoting the latitudes at which eruptions occur with the progress of the solar cycle. With a meridional circulation confined to the tachocline and above (**A**), the strongest magnetic fields form at high latitudes, resulting in eruptions there. With a meridional flow that penetrates below the tachocline (**B**) (streamlines of such a flow are shown in Fig. 3A), the above scenario changes, resulting in eruptions only at low latitudes, as observed. A deeply penetrating flow increases the dynamo time period. For example, the half-cycle period for (A) is about 15 years, whereas that of (B) is 18 years. Although the parameters can be fine-tuned to reduce the period, we do not attempt this, as we are interested in the robust large-scale behavior.

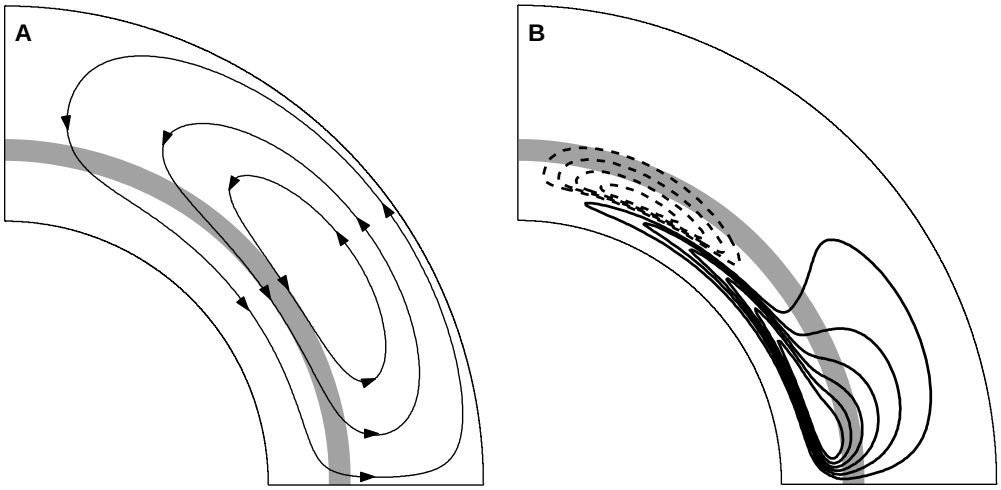

Fig. 3. A meridional cut of the Sun corresponding to the simulation geometry (the same domain as in Fig. 1). The meridional circulation (**A**) is depicted by black streamlines with arrows marking the direction of flow. The flow now penetrates below the tachocline (the shaded gray region) down to a depth of 0.6*R*. A snapshot of the toroidal field configuration at a particular instant of time (**B**) shows a belt of negative toroidal field (dashed contours) being pushed below the tachocline (into the stable region) by the penetrating flow at high latitudes, while simultaneously at low latitudes, a belt of positive toroidal field (solid contours) is being pushed out into the convection zone, where it can erupt to form sunspots.

mechanism can drive such a deeply penetrating meridional flow. However, recent simulations of solar convection show that downward-directed convective plumes (originating in the SCZ and penetrating into the stable regions below) tend to have a net equatorward motion inside the stable region (*27, 28*). These downward plumes are capable of pushing the magnetic field into the stable interior (*29*).

We have shown that a meridional circulation penetrating below the tachocline can explain the latitudinal distribution of sunspots. At present, this seems the best way to resolve the impasse that has been plaguing modern solar dynamo theory. Although the ill-understood question of angular momentum balance (*30*) must be addressed for a flow penetrating into the nearly uniformly rotating upper radiative region, this flow would help in explaining the lithium depletion and its connection to angular momentum loss (*31*) observed in stars at various phases of stellar evolution. A penetrating flow can also contribute to the sound speed anomaly that is observed beneath the tachocline (*32, 33*).

References and Notes

1. S. H. Schwabe, *Astron. Nachr.* **21**, 2 (1844).
2. G. E. Hale, *Astrophys. J.* **28**, 315 (1908).
3. E. N. Parker, *Astrophys. J.* **122**, 293 (1955).
4. _____, *Cosmical Magnetic Fields* (Clarendon, Oxford, 1979).
5. A. R. Choudhuri, *The Physics of Fluids and Plasmas: An Introduction for Astrophysicists* (Cambridge Univ. Press, Cambridge, 1998).
6. J. Schou *et al.*, *Astrophys. J.* **505**, 390 (1998).
7. P. Charbonneau *et al.*, *Astrophys. J.* **527**, 445 (1999).
8. A. R. Choudhuri, P. A. Gilman, *Astrophys. J.* **316**, 788 (1987).
9. S. D'Silva, A. R. Choudhuri, *Astron. Astrophys.* **272**, 621 (1993).
10. Y. Fan, G. H. Fisher, E. E. DeLuca, *Astrophys. J.* **405**, 390 (1993).
11. H. W. Babcock, *Astrophys. J.* **133**, 572 (1961).
12. R. B. Leighton, *Astrophys. J.* **156**, 1 (1969).
13. A. R. Choudhuri, M. Schüssler, M. Dikpati, *Astron. Astrophys.* **303**, L29 (1995).
14. M. Dikpati, P. Charbonneau, *Astrophys. J.* **518**, 508 (1999).
15. M. Küker, G. Rüdiger, M. Schultz, *Astron. Astrophys.* **374**, 301 (2001).
16. D. Nandy, A. R. Choudhuri, *Astrophys. J.* **551**, 576 (2001).
17. Y.-M. Wang, N. R. Sheeley, A. G. Nash, *Astrophys. J.* **383**, 431 (1991).
18. B. R. Durney, *Sol. Phys.* **160**, 213 (1995).
19. _____, *Astrophys. J.* **486**, 1065 (1997).
20. P. M. Giles, T. L. Duvall, P. H. Scherrer, R. S. Bogart, *Nature* **390**, 52 (1997).
21. D. C. Braun, Y. Fan, *Astrophys. J.* **508**, L105 (1998).
22. Methods are available as supporting material on *Science* Online.
23. J. A. Markiel, J. H. Thomas, *Astrophys. J.* **523**, 827 (1999).
24. D. Nandy, A. R. Choudhuri, in preparation.
25. E. A. Spiegel, N. O. Weiss, *Nature* **287**, 616 (1980).
26. A. A. Van Ballegooijen, *Astron. Astrophys.* **113**, 99 (1982).
27. N. H. Brummell, N. E. Hurlburt, J. Toomre, *Astrophys. J.* **493**, 955 (1998).
28. M. S. Miesch *et al.*, *Astrophys. J.* **532**, 593 (2000).
29. S. M. Tobias, N. H. Brummell, T. L. Clune, J. Toomre, *Astrophys. J.* **549**, 1183 (2001).
30. B. R. Durney, *Astrophys. J.* **528**, 486 (2000).
31. J.-P. Zahn, *Astron. Astrophys.* **265**, 115 (1992).
32. A. G. Kosovichev *et al.*, *Sol. Phys.* **170**, 43 (1997).
33. J. R. Elliot, D. O. Gough, *Astrophys. J.* **516**, 475 (1999).

34. We thank B. Durney, M. Miesch, A. Kosovichev, P. Scherrer, and H. M. Antia for critical discussions on various aspects of the present study.

Supporting Online Material

www.sciencemag.org/cgi/content/full/296/5573/1671/DC1
Methods

15 February 2002; accepted 17 April 2002

Biodegradable, Elastic Shape-Memory Polymers for Potential Biomedical Applications

Andreas Lendlein[1]* and Robert Langer[2]

The introduction of biodegradable implant materials as well as minimally invasive surgical procedures in medicine has substantially improved health care within the past few decades. This report describes a group of degradable thermoplastic polymers that are able to change their shape after an increase in temperature. Their shape-memory capability enables bulky implants to be placed in the body through small incisions or to perform complex mechanical deformations automatically. A smart degradable suture was created to illustrate the potential of these shape-memory thermoplastics in biomedical applications.

Current approaches for implanting medical devices, many of which are polymeric in nature, often require complex surgery followed by device implantation. With the advent of minimally invasive surgery (*1*), it is possible to place small devices with laprascopes. Such advances create new opportunities but also new challenges. How does one implant a bulky device or knot a suture in a confined space? It occurred to us that the creation of biocompatible (and ideally in many cases degradable) shape-memory polymers with the appropriate mechanical properties might enable the development of novel types of medical devices.

Shape-memory polymers possess the ability to memorize a permanent shape that can substantially differ from their initial temporary shape. Large bulky devices could thus potential-

[1]mnemoScience GmbH, Pauwelsstraβe 19, D-52074 Aachen, and Institute for Technical and Macromolecular Chemistry, RWTH Aachen, Germany. [2]Department of Chemical Engineering, Massachusetts Institute of Technology, 45 Carleton Street, Cambridge, MA 02139, USA.

*To whom correspondence should be addressed. E-mail: a.lendlein@mnemoscience.de